Journal of Computational Physics 228 (2009) 6682–6702

Contents lists available at ScienceDirect

Journal of Computational Physics

journal homepage: www.elsevier.com/locate/jcp

High-order well-balanced schemes and applications to non-equilibrium flow ☆

Wei Wang [a], Chi-Wang Shu [b,*], H.C. Yee [c], Björn Sjögreen [d]

[a] Center for Turbulence Research, Stanford University, Stanford, CA 94305, United States
[b] Division of Applied Mathematics, Brown University, Providence, RI 02912, United States
[c] NASA Ames Research Center, Moffett Field, CA 94035, United States
[d] Lawrence Livermore National Laboratory, Livermore, CA 94551, United States

ARTICLE INFO

Article history:
Received 12 February 2009
Received in revised form 13 May 2009
Accepted 14 May 2009
Available online 27 May 2009

Keywords:
Well-balanced schemes
Non-equilibrium flow
Chemical reactions
WENO schemes
TVD schemes
Nozzle flow

ABSTRACT

The appearance of the source terms in modeling non-equilibrium flow problems containing finite-rate chemistry or combustion poses additional numerical difficulties beyond that for solving non-reacting flows. A well-balanced scheme, which can preserve certain non-trivial steady state solutions exactly, may help minimize some of these difficulties. In this paper, a simple one-dimensional non-equilibrium model with one temperature is considered. We first describe a general strategy to design high-order well-balanced finite-difference schemes and then study the well-balanced properties of the high-order finite-difference weighted essentially non-oscillatory (WENO) scheme, modified balanced WENO schemes and various total variation diminishing (TVD) schemes. The advantages of using a well-balanced scheme in preserving steady states and in resolving small perturbations of such states will be shown. Numerical examples containing both smooth and discontinuous solutions are included to verify the improved accuracy, in addition to the well-balanced behavior.

1. Introduction

In the modeling of unsteady reactive problems, the interaction of turbulence with finite-rate chemistry introduces a wide range of space and time scales, leading to additional numerical difficulties. A main difficulty stems from the fact that most numerical algorithms used in reacting flows were originally designed to solve non-reacting fluids. As a result, spatial stiffness due to the reacting source terms and turbulence/chemistry interaction are major stumbling blocks to numerical algorithm development. One of the important numerical issues is the improper numerical treatment of a system of highly coupled stiff non-linear source terms, which will result in possible spurious steady state numerical solutions (see Lafon and Yee [14,15]). It was also shown in Lafon and Yee [14,15] that various ways of discretizing the reaction term and initial data can affect the stability of, and convergence to, the spurious numerical steady states and/or the exact steady states. Pointwise evaluation of the source terms appears to be the least stable (see [2,6,14,15]).

A well-balanced scheme (for time-dependent PDEs), as coined by LeVeque [16], which can preserve certain nontrivial steady state solutions exactly, may help minimize some of the spurious numerical behavior. Furthermore, well-balanced schemes capture small perturbations of the steady state solutions with high accuracy, thereby making them well suited for computations of turbulent fluctuations on a mainly steady flow field. While general schemes can only resolve perturba-

☆ This paper is an expanded version of "On well-balanced schemes for non-equilibrium flow with stiff source terms" in Stanford CTR Annual Research Briefs 2008.

* Corresponding author. Tel.: +1 401 863 2549; fax: +1 401 863 1355.
E-mail address: shu@dam.brown.edu (C.-W. Shu).

0021-9991/$ - see front matter © 2009 Elsevier Inc. All rights reserved.
doi:10.1016/j.jcp.2009.05.028

tions at the level of truncation error with the specific grid, well-balanced schemes can resolve much smaller perturbations, usually at 1% or lower of the main steady state flow. Most work about well-balanced schemes developed in the literature is for the shallow water equations (e.g. [5,8,9,11,13,19–21,23,28,35]). We follow the work by Xing and Shu in 2005 [26]. They develop a well-balanced high-order finite-difference weighted essentially non-oscillatory (WENO) scheme for solving the shallow water equations, which is non-oscillatory, well-balanced for still water, and genuinely high-order in smooth regions. In [27], they generalize the high order well-balanced WENO scheme to solve a wider class of hyperbolic systems with separable source terms.

In this paper, we apply their approach to construct a high-order well-balanced WENO scheme for the equations of non-equilibrium flow with reaction terms in one space dimension. Generalizations to multi-dimension can be done following the procedure given in [26] for the shallow water equations. Work in this area is forthcoming.

The one-dimensional hyperbolic system of conservation laws with source terms (also called a balance law)

$$U_t + F(U,x)_x = S(U,x), \tag{1}$$

is considered, where U is the solution vector, $F(U,x)$ is the convective flux and $S(U,x)$ is the source term. This balance law admits steady state solutions in which the source term is exactly balanced by the flux gradient. The objective of well-balanced schemes is to preserve exactly some of these steady state solutions. In non-equilibrium flow containing finite-rate chemistry, the source term represents the production of species from chemical reactions. One important property of this type of source term for non-equilibrium flow (which may make the work easier) is that x does not appear explicitly in $S(U,x)$, i.e., $S(U,x) \equiv S(U)$.

The well-balanced property of various popular linear and non-linear numerical schemes in the literature is studied in this paper based on a simple one-dimensional model with one temperature and three species (O_2, O and N_2). This model is obtained by reducing the model by Gnoffo et al. [4]. The different behaviors of those numerical schemes in preserving steady states and in resolving small perturbations of such states will be shown. High-order well-balanced WENO schemes are also designed and applied to the one-dimensional model. The procedure of designing well-balanced schemes presented here is valid for any number of species, although the numerical simulations are only performed for the three species model.

We will show that for the stationary steady state solutions of the reactive flow, the well-balanced schemes will give machine round-off errors regardless of the mesh sizes, while the non well-balanced schemes give truncation errors consistent with the formal order of accuracy for the schemes. Well-balanced schemes can resolve small perturbations of such steady state solutions well with very coarse meshes, while the non well-balanced schemes would give spurious structures in the numerical solutions, which will decrease and eventually disappear with a mesh refinement. Our work indicates the advantage of well-balanced schemes: they can be used to resolve small perturbations of the steady state solutions, e.g., turbulent fluctuations, using much coarser meshes than that for the non well-balanced schemes, thereby saving a lot of CPU time, especially when the number of species increases.

Numerical tests also include high-temperature shock tube and nozzle flows. It will be shown that the well-balanced schemes will not lose any accuracy or other good properties such as non-oscillatory shock-capturing for approximating solutions away from the steady state.

2. Governing equations

Assuming no conduction or radiation, the considered non-equilibrium models are a system of hyperbolic conservation laws with source terms, denoted by

$$U_t + F(U)_x = S(U). \tag{2}$$

Here $U, F(U)$ and $S(U)$ are column vectors with $m = n_s + 2$ components where n_s is the number of species

$$U = (\rho_1, \ldots, \rho_{n_s}, \rho v, \rho e_0)^T, \tag{3}$$

$$F(U) = (\rho_1 v, \ldots, \rho_{n_s} v, \rho v^2 + p, \rho v e_0 + v p)^T, \tag{4}$$

$$S(U) = (s^1, \ldots, s^{n_s}, 0, 0)^T, \tag{5}$$

where ρ_s is the density of species s, v is the velocity and e_0 is the internal energy per unit mass of the mixture. The total density is defined as $\rho = \sum_{s=1}^{n_s} \rho_s$ and the pressure p is given by

$$p = RT \sum_{s=1}^{n_s} \frac{\rho_s}{M_s}, \tag{6}$$

where R is the universal gas constant and M_s is the molar mass of species s. The temperature T can be found from the total energy

$$\rho e_0 = \sum_{s=1}^{n_s} \rho_s e_{i,s}(T) + \sum_{s=1}^{n_s} \rho_s h_s^0 + \frac{1}{2}\rho v^2, \tag{7}$$

where $e_{i,s} = C_{v,s}T$ is the internal energy with $C_{v,s} = 3R/2M_s$ and $5R/2M_s$ for monoatomic species and diatomic species, respectively, and the enthalpies h_s^0 are constants.

The source term $S(U)$ describes the chemical reactions occurring in gas flows which result in changes in the amount of mass of each chemical species. We assume there are J reactions of the form

$$\nu'_{1j}X_1 + \nu'_{2j}X_2 + \ldots + \nu'_{n_s j}X_{n_s} \rightleftharpoons \nu''_{1j}X_1 + \nu''_{2j}X_2 + \ldots + \nu_{n_s j}X_{n_s}, \quad j = 1, \ldots, J, \tag{8}$$

where ν'_{1j} and ν''_{1j} are, respectively the stoichiometric coefficients of the reactants and products of species i in the jth reaction. For non-equilibrium chemistry, the rate of production of species i due to chemical reaction, may be written as

$$s^i = M_i \sum_{j=1}^{J} \left(\nu''_{i,j} - \nu'_{i,j}\right) \left[k_{f,j} \prod_{s=1}^{n_s} \left(\frac{\rho_s}{M_s}\right)^{\nu'_{s,j}} - k_{b,j} \prod_{s=1}^{n_s} \left(\frac{\rho_s}{M_s}\right)^{\nu''_{s,j}}\right], \quad i = 1, \ldots, n_s. \tag{9}$$

For each reaction j, the forward and backward reaction rates, $k_{f,j}$ and $k_{b,j}$ are assumed to be known functions of the temperature.

Let us denote the Jacobian $A = \partial F/\partial U$ with $(a^1, \ldots, a^m)$ being the eigenvalues of A,

$$(a^1, \ldots, a^m) = (v, \ldots, v, v + a, v - a), \tag{10}$$

where a is the so-called "frozen speed of sound". Denote R as the matrix whose columns are eigenvectors of A (not to be confused with the R in Eq. (6)). Let $a^l_{j+1/2}, R_{j+1/2}$ denote the quantities a^l and R evaluated at some symmetric average of U_j and U_{j+1}, such as Roe's average [22]. Define

$$\alpha_{j+1/2} = R^{-1}_{j+1/2}(U_{j+1} - U_j) \tag{11}$$

as the difference of the local characteristic variables in the x direction.

In this paper, the considered schemes are the fifth-order finite-difference WENO schemes [10,24], second-order semi-implicit predictor–corrector total variation diminishing (TVD) scheme (P–C TVD) [17,32], second-order symmetric TVD scheme [29] and Harten and Yee TVD scheme [30,31] and second-order MUSCL scheme [30]. Except for the P–C TVD scheme, the explicit TVD high-order Runge–Kutta method [25] as well as the pointwise implicit additive Runge–Kutta (ARK) method [12] are used for time discretization (see Appendix A for more details).

3. Well-balanced WENO schemes and linear schemes

A well-balanced scheme refers to a scheme that preserves exactly specific steady state solutions of the governing equations.

We will first consider the 1D scalar balance law

$$u_t + f(u,x)_x = s(u,x), \tag{12}$$

i.e., the steady state solution u satisfying

$$f(u,x)_x = s(u,x). \tag{13}$$

Here lowercase letters "f", "u" and "s" are used to denote scalar quantities and scalar functions, to distinguish them from the uppercase letters "F", "U" and "S" for the system case.

A linear finite-difference operator D is defined to be one satisfying $D(af_1 + bf_2) = aD(f_1) + bD(f_2)$ for constants a, b and arbitrary grid functions f_1 and f_2. A scheme for Eq. (12) is said to be a linear scheme if all the spatial derivatives are approximated by linear finite-difference operators.

Xing and Shu [27] proved that under the following two assumptions regarding Eq. (12) and the steady state solution of Eq. (13), linear schemes with certain restrictions are well-balanced schemes. Furthermore, high-order non-linear WENO schemes can be adapted to become well-balanced schemes.

Assumption 1. The considered steady state preserving solution u of Eq. (13) satisfies

$$r(u,x) = constant, \tag{14}$$

for a known function $r(u,x)$.

Assumption 2. The source term $s(u,x)$ can be decomposed as

$$s(u,x) = \sum_i \tau_i(r(u,x))t'_i(x), \tag{15}$$

for a finite number of functions τ_i and t_i. (Here t_i is not to be confused with the time "t" indicated on all previous conservation laws.)

We remark that the non-equilibrium flow including nozzle flow studied later in this paper does satisfy these assumptions. A linear scheme applied to Eq. (13) would have a truncation error

$$D(f(u,x)) - \sum_i \tau_i(r(u,x))D_i(t_i(x)), \tag{16}$$

where D and D_i are linear finite-difference operators used to approximate the spatial derivatives. One restriction to the linear schemes is needed:

$$D_i = D \quad \text{for all} \quad i \tag{17}$$

when applied to the steady state solution. For such linear schemes we have

Proposition 1. *For the balance law Eq. (12) with source term Eq. (15), linear schemes with the restriction Eq. (17) for the steady state solutions satisfying Eq. (14) are well-balanced schemes.*

Proof. For the steady state solutions satisfying Eq. (14), the truncation error for such linear schemes with Eq. (17) reduces to

$$D(f(u,x)) - \sum_i \tau_i(r(u,x))D(t_i(x)) = D\left(f(u,x) - \sum_i \tau_i(r(u,x))t_i(x)\right),$$

where the linearity of D and the fact that $r(u,x)$ is constant for the steady state solution u are used. Note that for such steady state solution $u, f(u,x) - \sum_i \tau_i(r(u,x))t_i(x)$ is a constant, because

$$\frac{d}{dx}\left(f(u,x) - \sum_i \tau_i(r(u,x))t_i(x)\right) = f(u,x)_x - \sum_i \tau_i(r(u,x))t_i'(x) = f(u,x)_x - s(u,x) = 0.$$

Thus, the truncation error is zero for any consistent finite-difference operator D. Therefore, linear schemes with Eq. (17) preserve these steady state solutions exactly. □

Now the high-order non-linear finite-difference WENO schemes are considered in which the non-linearity comes from the non-linear weights and the smoothness indicators. We follow the procedures described in Xing and Shu [26,27] for the shallow water equations. The description below is brief, for better understanding of notations and terminologies we refer to [10,24]. First, for the situation without flux splitting (19), e.g., for the WENO-Roe scheme defined in [10], the WENO approximation to f_x can be written as

$$f_x|_{x=x_j} \approx \sum_{k=-r}^{r} c_k f_{k+j} = D_f(f)_j,$$

where $r = 3$ for the fifth-order WENO approximation and the coefficients c_k depend non-linearly on the smoothness indicators involving the grid function $f_{j-r}, \ldots, f_{j+r}$. The key idea now is to use the finite-difference operator D_f, and apply it to approximate $t_i'(x)$ in the source terms (see also [20,21]), i.e.,

$$t_i'(x_j) \approx \sum_{k=-r}^{r} c_k t_i(x_{k+j}) = D_f(t_i(x))_j. \tag{18}$$

The finite-difference operator D_f is obtained from the high-order WENO procedure. Even though its coefficients depend non-linearly on f, when f is smooth, these coefficients are sufficiently close to those of the linear high-order scheme, so that D_f acting on any smooth function approximates the first derivative of that function to high-order. Clearly, the condition for the proof of Proposition 1 is now satisfied and we conclude that the high-order finite-difference WENO scheme as stated above, without the flux splitting, and with the special handling of the source terms described above, maintains exactly the steady state.

Next, WENO schemes with a Lax–Friedrichs flux splitting, such as WENO-LF and WENO-LLF, are considered. The flux $f(u,x)$ is written as a sum of $f^+(u,x)$ and $f^-(u,x)$, defined by

$$f^{\pm}(u) = \frac{1}{2}(f(u) \pm \alpha u), \tag{19}$$

where α is taken as $\alpha = \max_u |f'(u)|$. The main obstacle to achieve a well-balanced scheme for this case is the appearance of the artificial viscosity term $\pm\alpha u$, which leads to a non-zero truncation error at steady state since the solution u is not a polynomial. In order to obtain a well-balanced scheme, the $\pm\alpha u$ term in the Lax-Friedrichs flux splitting (19) is replaced by

$$\pm\alpha' \ \mathrm{sgn}\left(\frac{\partial r(u,x)}{\partial u}\right) r(u,x), \tag{20}$$

where "sgn" is the sign function with values +1 or −1. Basically, the dissipation difference caused by (19), given by

$$\alpha(u^+ - u^-), \tag{21}$$

where u^- and u^+ refer to the left-biased and right-biased approximations to the value of u at the interface where the numerical flux is needed, is replaced by

$$\alpha'(r(u^+,x)-r(u^-,x)), \tag{22}$$

in (20) if we assume the "sgn" term is +1. By the mean value theorem applied to (22), $\alpha'\frac{\partial r}{\partial u}(\xi,x)$ in (22), where ξ is between u^- and u^+, corresponds to the constant α in (21). Of course, we would need to assume that $\frac{\partial r(u,x)}{\partial u}$ does not change sign within the local region. We would suitably adjust the size of α' in (22) by the size of $\frac{\partial r(u,x)}{\partial u}$ (some local average of it), so that dissipation effects of (21) and (22) are close. We refer to [27] for more details. Notice that now the artificial viscosity term $\pm r(u,x)$ is constant at the specific steady state by (14), resulting in a zero truncation error for its difference and hence well-balancedness.

The framework described for the scalar case can be easily applied to systems (1). For a system with m equations, we would have m relationships in the form of Eq. (14):

$$r_l(U,x)=\text{constant},\quad l=1,\ldots,m. \tag{23}$$

In Assumption 2, τ_i could be arbitrary functions of $r_l(U,x)$, and τ_i and t_i can be different for different components of the source vector. The characteristic decomposition procedure for WENO schemes does not alter the argument presented for the scalar case (see [26]). The modified WENO schemes through the procedure above will maintain exactly the steady state and will be called "balanced WENO" schemes below.

However, the modification of the viscosity coefficient α in the Lax–Friedrichs building block in order to obtain well-balancedness for the steady state may adversely affect stability near strong shocks for solutions far away from the steady state, if Eq. (20) is used to obtain the well-balanced WENO-LF scheme for the system case. Here an equilibrium limiter is introduced, similar to the one used in [18], to determine whether the region is near or far away from the steady state. The Lax–Friedrichs flux splitting (19) is changed to

$$f^{\pm}(u)=\frac{1}{2}(f(u)\pm\alpha\lambda u), \tag{24}$$

with

$$\begin{aligned}\lambda:=\max&\left(\min\left(1,\frac{(|r_1(U_{i+1},x_{i+1})-r_1(U_i,x_i)|+|r_1(U_{i-1},x_{i-1})-r_1(U_i,x_i)|)^2}{|r_1(U_{i+1},x_{i+1})-r_1(U_i,x_i)|^2+|r_1(U_{i-1},x_{i-1})-r_1(U_i,x_i)|^2+\varepsilon}\right),\ldots,\right.\\ &\left.\min\left(1,\frac{(|r_m(U_{i+1},x_{i+1})-r_m(U_i,x_i)|+|r_m(U_{i-1},x_{i-1})-r_m(U_i,x_i)|)^2}{|r_m(U_{i+1},x_{i+1})-r_m(U_i,x_i)|^2+|r_m(U_{i-1},x_{i-1})-r_m(U_i,x_i)|^2+\varepsilon}\right)\right),\end{aligned} \tag{25}$$

where ε is a small number to avoid zero in the denominator and we take it as 10^{-6} in the computation. Near the specific steady state, the differences in r_i shown in (25) are close to zero. λ will be near zero when all these differences are small compared with ε. λ is near one if the solution is far from the steady state, since the differences in r_i shown in (25) are now on the level of $O(\Delta x)$ and much larger than ε, and then the scheme is the regular WENO-LF scheme. The limiter does not affect the high-order accuracy of the scheme in smooth region for general solutions of Eq. (2). In the specific steady state, since all the r_l $(l=1,\ldots,m)$ are constants, λ returns zero and then the scheme maintains the exact solutions for such steady state. To avoid confusion with "balanced WENO" schemes mentioned above, the WENO-LF with the flux splitting (24) and the equilibrium limiter (25) will be called "hybrid WENO-LF".

Finally, the well-balanced properties of various TVD schemes mentioned in Section 2 will be investigated. The semi-implicit Predictor–Corrector TVD (P–C TVD) scheme [17,32] for Eq. (2) has the form

$$\left[1-\frac{1}{2}\Delta tS'(U_j^n)\right]\Delta U_j^{(1)}=-\frac{\Delta t}{\Delta x}\left(F_j^n-F_{j-1}^n\right)+\Delta tS_j^n, \tag{26}$$

$$U_j^{(1)}=\Delta U_j^{(1)}+U_j^n, \tag{27}$$

$$\left[1-\frac{1}{2}\Delta tS'(U_j^n)\right]\Delta U_j^{(2)}=-\frac{\Delta t}{\Delta x}\left(F_{j+1}^{(1)}-F_j^{(1)}\right)+\Delta tS_j^n, \tag{28}$$

$$U_j^{(2)}=\Delta U_j^{(2)}+U_j^{(1)}, \tag{29}$$

$$U_j^{n+1}=U_j^n+\frac{1}{2}\left(\Delta U_j^{(1)}+\Delta U_j^{(2)}\right)+\left[R_{j+1/2}^{(2)}\Phi_{j+1/2}^{(2)}-R_{j-1/2}^{(2)}\Phi_{j-1/2}^{(2)}\right]. \tag{30}$$

The third step Eq. (30) acts as a non-linear filter step [33]. The elements of the vector $\Phi_{j+1/2}$, denoted by $\phi_{j+1/2}^l$ with $l=1,\ldots m$ are

$$\phi_{j+1/2}^l=\frac{1}{2}\left[\psi(v_{j+1/2}^l)-(v_{j+1/2}^l)^2\right]\left(\alpha_{j+1/2}^l-\widehat{Q}_{j+1/2}^l\right), \tag{31}$$

where

$$v_{j+1/2}^l=\frac{\Delta t}{\Delta x}a_{j+1/2}^l. \tag{32}$$

The function $\psi(z)$ is an entropy correction to $|z|$. One possible form is ([30])

$$\psi(z) = \begin{cases} |z| & |z| \geqslant \delta_1, \\ (z^2 + \delta_1^2)/2\delta_1 & |z| < \delta_1, \end{cases} \tag{33}$$

where δ_1 is the entropy fix parameter. See [34] for a discussion. $\widehat{Q}^l_{j+1/2}$ is an unbiased limiter function which can be

$$\widehat{Q}^l_{j+1/2} = \text{minmod}\left(\alpha^l_{j-1/2}, \alpha^l_{j+1/2}\right) + \text{minmod}\left(\alpha^l_{j+1/2}, \alpha^l_{j+3/2}\right) - \alpha^l_{j+1/2}, \tag{34}$$

with

$$\text{minmod}(a,b) = \text{sgn}(a) \cdot \max\{0, \min[|a|, b\,\text{sgn}(a)]\}. \tag{35}$$

In this study, only diffusive limiters are considered. If a "smooth" limiter is preferred, then the minmod function minmod (a,b) is replaced by the following smooth function

$$g(a,b) = \left[a(b^2 + \delta_2) + b\left(a^2 + \delta_2\right)\right]/(a^2 + b^2 + 2\delta_2), \tag{36}$$

where δ_2 is a small parameter between 10^{-7} to 10^{-5}. The predictor step Eq. (26) and the corrector step Eq. (28) are linear. However, the last filter step is not linear. We will explore this further in the next section. Note that the accuracy of the scheme (and the two considered TVD and MUSCL schemes) reflects the choice of the very diffusive limiter. Numerical accuracy can be improved with a less diffusive limiter.

The numerical flux $\widehat{F}_{j+1/2}$ for the second-order symmetric TVD scheme [29] is described as

$$\widehat{F}_{j+1/2} = \frac{1}{2}(F_j + F_{j+1} + R_{j+1/2}\Phi_{j+1/2}), \tag{37}$$

where

$$\phi^l_{j+1/2} = -\psi\left(a^l_{j+1/2}\right)\left(\alpha^l_{j+1/2} - \widehat{Q}^l_{j+1/2}\right). \tag{38}$$

Pointwise evaluation to the source term is enough for the accuracy for the symmetric TVD scheme and also for the two TVD schemes in the following. Similar to P–C TVD, the non-linearity of the TVD scheme comes from the $\widehat{Q}^l_{j+1/2}$ part of the numerical flux Eq. (38).

The second-order Harten–Yee scheme [30,31] has the same form as Eq. (37) with

$$\phi^l_{j+1/2} = \frac{1}{2}\psi\left(a^l_{j+1/2}\right)\left(g^l_j + g^l_{j+1}\right) - \psi\left(a^l_{j+1/2} + \gamma^l_{j+1/2}\right)\alpha^l_{j+1/2}, \tag{39}$$

where

$$\gamma^l_{j+1/2} = \frac{1}{2}\psi\left(a^l_{j+1/2}\right)\begin{cases} \left(g^l_{j+1} - g^l_j\right)/\alpha^l_{j+1/2} & \alpha^l_{j+1/2} \neq 0, \\ 0 & \alpha^l_{j+1/2} = 0. \end{cases} \tag{40}$$

Examples of the limiter function g^l_j can be

$$g^l_j = \text{minmod}\left(\alpha^l_{j-1/2}, \alpha^l_{j+1/2}\right), \tag{41}$$

or the smooth Eq. (36).

Unlike P–C TVD and the TVD schemes, the second-order MUSCL scheme [30] is fully non-linear. The numerical flux for a MUSCL approach is expressed as

$$\widehat{F}_{j+1/2} = \frac{1}{2}\left(F\left(U^R_{j+1/2}\right) + F\left(U^L_{j+1/2}\right) - \widehat{R}_{j+1/2}\widehat{\Phi}_{j+1/2}\right), \tag{42}$$

with

$$U^R_{j+1/2} = U_{j+1} - \frac{1}{2}\Delta_{j+1}, \tag{43}$$

and

$$U^L_{j+1/2} = U_j + \frac{1}{2}\Delta_j. \tag{44}$$

The limiters can be

$$\Delta_j = \text{minmod}(U_{j+1} - U_j, U_j - U_{j-1}), \tag{45}$$

or the smooth Eq. (36). We can see that $U^R_{j+1/2}$ and $U^L_{j+1/2}$ bring non-linearity into every term of the flux Eq. (42).

4. Numerical study

This section presents several numerical examples of two types of flows with non-equilibrium chemistry, i.e., Euler flow with reactions and nozzle flow. Three test examples will be performed for each flow type. The first example is to numerically verify whether the considered schemes are well-balanced by time-marching on a nontrivial steady state. In this test, the well-balanced schemes which preserve the steady state solutions exactly will give round-off numerical errors. Next, this steady state is subject to small perturbations of different variables. From the numerical behavior of all the considered schemes, we can observe the well-balanced schemes showing their advantage in resolving the perturbations while the non well-balanced schemes will give spurious numerical truncation errors. The third example is a shock tube problem to test the shock-capturing capability of the considered schemes. We want to demonstrate that well-balanced schemes will not destroy the non-oscillatory shock resolution away from the steady state.

4.1. Three species model

In all test cases, a simple model for air involving 3 species, O_2, O and N_2 ($\rho_1 = \rho_{O_2}, \rho_2 = \rho_O$ and $\rho_3 = \rho_{N_2}$) is used. The model has reactions:

$$O_2 + M \rightleftharpoons O + O + M, \tag{46}$$

where M is a catalytic particle (any of the species present).

From Eq. (9), the source term $S(U)$ can be written as

$$S(U) = (2M_1\omega, -M_2\omega, 0, 0, 0), \tag{47}$$

with

$$\omega = \left(k_f(T)\frac{\rho_2}{M_2} - k_b(T)\left(\frac{\rho_1}{M_1}\right)^2\right)\left(\frac{\rho_1}{M_1} + \frac{\rho_2}{M_2} + \frac{\rho_3}{M_3}\right). \tag{48}$$

The forward reaction rate is

$$k_f = CT^{-2}e^{-E/T}, \tag{49}$$

where $C = 2.9 \times 10^{17}$ m^3 mole^{-1} s^{-1} and $E = 59750$ K (The unit "m" is short for meter, "s" is for second and "K" is for kelvin). The backward reaction rate is

$$k_b = k_f/k_{eq}, \tag{50}$$

with

$$k_{eq} = \exp(b_1 + b_2\log z + b_3 z + b_4 z^2 + b_5 z^3), \quad z = 10,000/T, \tag{51}$$

where the constants b_k are found in [4].

The steady state is of course not unique. In this paper we consider the special steady states with zero velocity and preserved chemical equilibrium. Then the flux in Eq. (2) is

$$F(U) = \begin{pmatrix} \rho_1 v \\ \rho_2 v \\ \rho_3 v \\ \rho v^2 + p \\ (\rho e_0 + p)v \end{pmatrix} = \begin{pmatrix} 0 \\ 0 \\ 0 \\ p \\ 0 \end{pmatrix}.$$

Since the chemical equilibrium condition $S(U) = 0$ implies $F(U)$ is a constant, we deduce that the pressure p is a constant in this case. Therefore, a set of conditions for such steady state is

$$\begin{cases} v = 0, \\ p = \text{constant}, \\ S(U) = 0. \end{cases} \tag{52}$$

Thus we can choose

$$r = S(U) = \text{constant}, \tag{53}$$

which is of the form (23). Note that x does not appear explicitly in $S(U)$, which makes the procedure simpler because all the $t_i'(x) = 1$ and the finite-difference operators D_i mentioned in Eq. (16) are absent. Therefore, as described in Section 3, linear schemes and WENO-Roe schemes applied to the specific steady state solution Eq. (52) for the problem Eq. (2) are well-balanced and maintain the original high-order accuracy. WENO-LF, WENO-LLF schemes with suitable modification as described in the previous section are also well-balanced and maintain the original high-order accuracy.

4.1.1. Well-balanced test

The purpose of the first test problem is to numerically verify whether the considered schemes are well-balanced for the special stationary case Eq. (52) with

$$\rho_O = 4 \times 10^{-5}(1 + 0.2\sin(5\pi x)) \text{ kg/m}^3, \quad p = 10^5 \text{ N/m}^2, \quad v = 0 \text{ m/s}, \tag{54}$$

with ρ_{O_2} and ρ_{N_2} obtained by the equilibrium state condition (The unit "kg" is for kilogram and "N" is for newton). We consider the air which consists of 21% of oxygen and 79% of nitrogen. This can be expressed as

$$\frac{\rho_O}{2M_O} + \frac{\rho_{O_2}}{M_{O_2}} = \frac{21}{79}\frac{\rho_{N_2}}{M_{N_2}}, \tag{55}$$

which holds for the equilibrium state. In the equilibrium state, since there is no reaction, the species also satisfy the source term $S(U) = 0$. This set of steady state solutions is of the form Eq. (52). Notice that the solutions are not constants or polynomials, making well-balancedness (zero truncation errors for such solutions) non-trivial. Eq. (54) is chosen as the initial condition which is also the exact steady state solution, and the results are obtained by time-accurate time-marching on the steady state. The relative L_1 error is measured to be the difference between the exact solution Eq. (54) and the numerical solution divided by the L_1 norm of the exact solution.

The error and accuracy at $t = 0.01$ (about 20,000 time steps for $N = 160$ grid points) are listed in Tables 1 and 2. It shows that WENO-Roe, P–C TVD and TVD schemes are well-balanced schemes because they produce errors at the level of machine round-off errors in double precision. However, WENO-LF and MUSCL schemes are not well-balanced. The hybrid WENO-LF scheme as stated in Section 3 is also verified to be well-balanced. We remark that the superconvergence of the results for WENO-LF and MUSCL is due to the simple form of the steady state solutions.

Numerically P–C TVD and TVD schemes have been shown to be well-balanced for the steady state solution Eq. (52). Even though the non-linear term $R\Phi$ in the P–C TVD (Eq. (30)) and TVD schemes (Eqs. (37) and (42)) is not linear, we will explain why this part will not destroy the well-balanced property in these schemes. Since they have similar formulas, we will use the symmetric TVD scheme as the example.

We claim that the function $\Phi = 0$ for this particular steady state problem Eq. (52). This is due to the fact that v is equal to zero for the steady state solution. Recalling the eigenvalue a in Eq. (10), it is easy to see that only the last two entries a^{n_s+1} and a^{n_s+2} are non-zero. For the function ψ defined in Eq. (33), if the entropy parameter δ_1 is set to be zero, we will have $\psi(a^l) = |a^l|$. Therefore, $\phi^1, \ldots, \phi^{n_s}$ are always zeros. Note that for any $\delta_1 > 0$, P–C TVD and TVD schemes are not well-balanced.

Next, let us consider the factor $\alpha^l_{j+1/2} - \widehat{Q}^l_{j+1/2}$ in Eq. (31) or Eq. (38), where $\alpha^l_{j+1/2}$ is given in Eq. (11).

The resulting equations are obtained directly from the system (see [7])

$$\alpha^{n_s+k} = (\Delta p \pm a\rho\Delta v)/2a^2 \quad k = 1, 2, \tag{56}$$

where α, v and the frozen speed of sound a are evaluated at the Roe average at $j + 1/2$, and $\Delta p = p_{j+1} - p_j$, etc. Since the pressure p is constant and velocity v is zero for the steady state solution, α^{n_s+1} and α^{n_s+2} are exactly zeros.

Hence, the non-linear term $R\Phi$ is zero and then the P–C TVD and TVD schemes become linear schemes for the steady state solution Eq. (52). By Proposition 1, they are well-balanced schemes towards the steady state solution (52).

Table 1
L^1 relative errors for ρ_o by WENO schemes with N uniform grid points.

N	Error	Error	Order	Error
	WENO-Roe	WENO-LF		Hybrid WENO-LF
40	7.18E−15	2.89E−05	–	6.95E−13
80	6.58E−15	2.83E−07	6.67	2.34E−13
160	8.81E−15	3.25E−09	6.45	1.50E−12

Table 2
L^1 relative errors for ρ_o by TVD schemes with minmod/smooth limiter with N uniform grid points, $\delta_1 = 0$.

N	Error	Error	Error	Error	Order
Minmod limiter	P–C TVD	symmetric TVD	Harten–Yee TVD	MUSCL	
40	1.23E−14	5.93E−17	5.93E−17	3.86E−05	–
80	1.10E−14	5.71E−17	9.95E−17	5.15E−06	3.25
160	1.14E−14	1.69E−17	1.93E−16	3.25E−07	3.98
Smooth limiter					
40	6.21E−15	5.50E−17	7.29E−15	5.03E−04	–
80	7.38E−15	6.14E−17	7.00E−15	2.25E−05	4.48
160	9.26E−15	1.81E−15	9.66E−15	4.14E−07	5.76

Table 3
Well-balanced property for WENO and second-order TVD schemes for zero velocity steady states of reactive Euler flows.

	WENO-Roe	WENO-LF	Hybrid WENO-LF	P–C TVD	Harten–Yee	MUSCL
Well-balanced	Yes	No	Yes	Yes	Yes	No

From both numerical tests and theoretical analysis, we can summarize the well-balanced properties of the considered schemes for the zero velocity steady states Eq. (52) in Table 3.

4.1.2. Small perturbation

The following test problems will demonstrate the advantages of well-balanced schemes through the problem of a small perturbation over a stationary state.

The same stationary state solution Eq. (54) is considered. First, a small perturbation $\epsilon = 10^{-10} \times \sin(\pi x)$ (about 0.001% of the mean flow) is added to the density, i.e.,

$$\rho_0' = \rho_0 + \epsilon. \tag{57}$$

The other quantities are kept unperturbed. At $t = 0.1$, the difference between the perturbed solutions of density ρ_0 and the steady state solutions of density ρ_0 is plotted ("Δ" denotes the "difference" in the figures). The reference results are computed by WENO-Roe with 1200 points and are considered to be "exact". To improve the viewing, a factor of 10^{10} is multiplied to all the figures.

The density ρ_0 by WENO-Roe is depicted in the left subplot of Fig. 1. The advantage of the well-balanced property of WENO-Roe is clearly demonstrated with only 100 points to resolve such small perturbation. Although the solution indicates two small bumps in the density plot, these bumps disappear when the mesh is refined to 200 points.

Unlike the well-behaved WENO-Roe, the results by WENO-LF, which is not a well-balanced scheme, behave in a very oscillatory fashion using 100 grid points (middle subplot of Fig. 1). This is due to the fact that the well-balanced schemes can resolve the steady state solution exactly, hence they are able to resolve a very small perturbation. However, a scheme that is not well-balanced can only resolve the solution when the mesh is refined enough such that the truncation error of the scheme is much smaller than the perturbation. For example, when the mesh is refined to 300 points for WENO-LF (middle subplot of Fig. 1), the oscillations disappear and the solution is resolved. The right subplot of Fig. 1 shows the good behavior of the hybrid WENO-LF scheme. It resolves the perturbation perfectly with only 100 points.

Next, the numerical results by P–C TVD, TVD and MUSCL schemes are discussed, respectively. As indicated in Section 4.1.1, P–C TVD and TVD schemes are well-balanced schemes for both the minmod limiter and the smooth limiter. The numerical results of P–C TVD and TVD schemes with the smooth limiter show very good agreement with the reference solution (right subplots of Figs. 2–4), whereas the MUSCL scheme, which is not well-balanced, exhibits oscillatory behavior (Fig. 5 right) for the same mesh $N = 300$.

However, note that in the left subplots of Figs. 2–4, results for P–C TVD and TVD schemes with the minmod limiter exhibit some oscillations. These oscillations do not disappear in the mesh refinement until the mesh is extremely fine. This might be caused by the lack of smoothness of the minmod limiter, which is continuous but not differentiable. For the sake of this, only the smooth limiter will be considered in the following test problems.

Next our schemes are tested on a perturbation of velocity and a perturbation of energy, i.e.

$$v' = v + \epsilon, \tag{58}$$

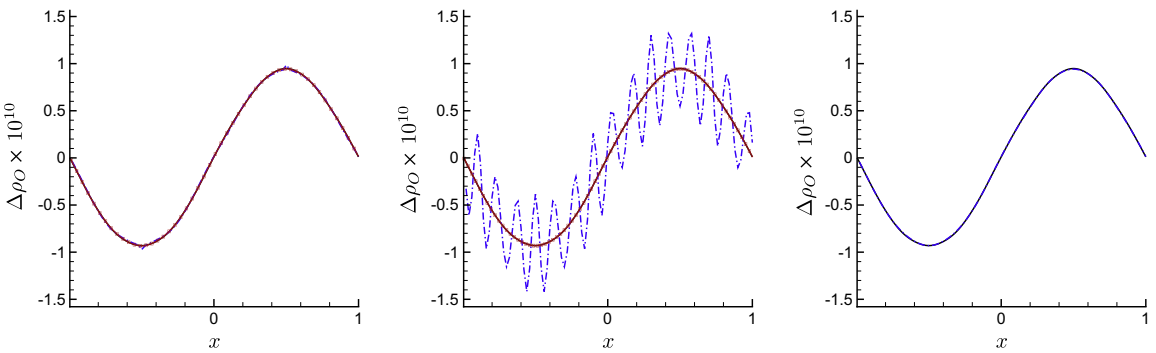

Fig. 1. Small perturbation of density results by WENO: $\epsilon = 10^{-10} \times \sin(\pi x)$. Left: WENO-Roe (WENO-Roe 100 points: dash-dot; WENO-Roe 200 points: dotted with symbols); middle: WENO-LF (WENO-LF 100 points: dash-dot; WENO-LF 300 points: dotted with symbols); right: hybrid WENO-LF (hybrid WENO-LF 100 points: dash-dot). Reference: WENO-Roe 1200 points: solid.

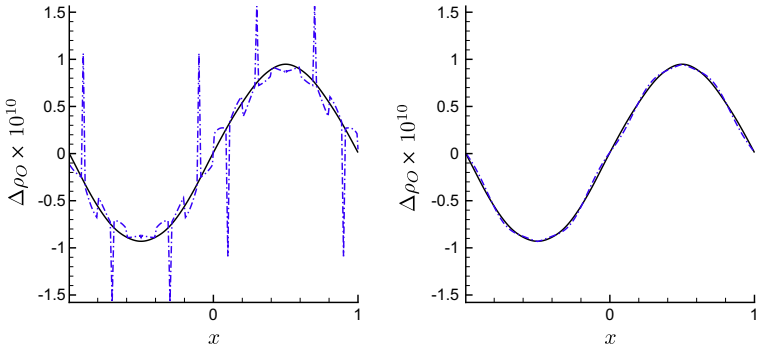

Fig. 2. Small perturbation of density results by P–C TVD: $\epsilon = 10^{-10} \times \sin(\pi x), \delta_1 = 0$. Left: with the minmod limiter; right: with the smooth limiter (P–C TVD 300 points: dash-dot; WENO-Roe 1200 points: solid).

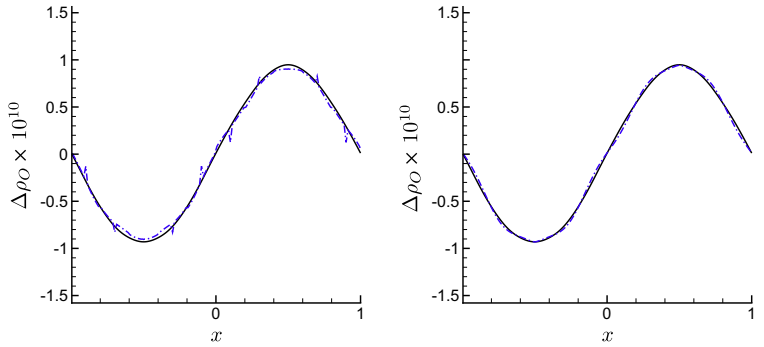

Fig. 3. Small perturbation of density results by symmetric TVD: $\epsilon = 10^{-10} \times \sin(\pi x), \delta_1 = 0$. Left: with the minmod limiter; right: with the smooth limiter (symmetric TVD 300 points: dash-dot; WENO-Roe 1200 points: solid).

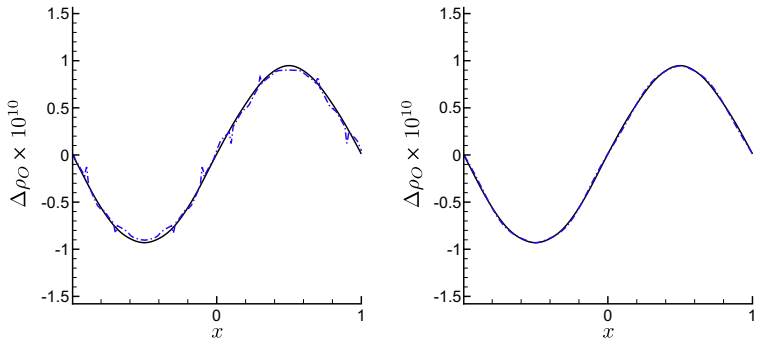

Fig. 4. Small perturbation of density results by Harten–Yee TVD: $\epsilon = 10^{-10} \times \sin(\pi x), \delta_1 = 0$. Left: with the minmod limiter; right: with the smooth limiter (Harten–Yee 300 points: dash-dot; WENO-Roe 1200 points: solid).

$$\rho e_0' = \rho e_0 + \epsilon, \tag{59}$$

both with $\epsilon = 10^{-3} \times \sin(\pi x)$. Similar to the density case, the difference of the perturbed solutions and the steady state solutions are plotted. But for the velocity case, since the steady state solution is zero, the velocity plots are the perturbed solution. Fig. 6 shows the velocity plot under a small perturbation of velocity (58) by WENO-Roe, WENO-LF and hybrid WENO-LF, respectively. The results by P–C TVD, Harten–Yee TVD and MUSCL are shown in Fig. 7. Figs. 8 and 9 show the energy plot under a small perturbation of energy (59) by three WENO schemes and three second-order TVD schemes, respectively. Again, the well-balanced schemes WENO-Roe (left subplots of Figs. 6 and 8), hybrid WENO-LF (right subplots of Figs. 6 and 8), P–C TVD (left subplots of Figs. 7 and 9), Harten–Yee TVD (middle subplots of Figs. 7 and 9) all show very good agreements with the reference solutions even in a coarse mesh. The results by regular WENO-LF (middle subplots of Figs. 6 and 8) have some oscillations in the coarse mesh due to the truncation errors. The results by MUSCL scheme (right subplots of Figs. 7 and 9)

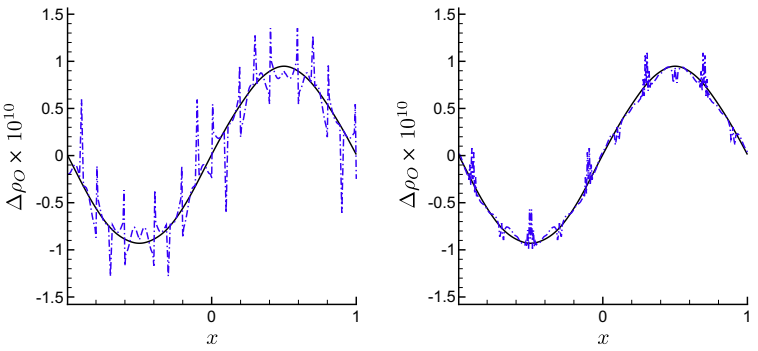

Fig. 5. Small perturbation of density results by MUSCL scheme: $\epsilon = 10^{-10} \times \sin(\pi x), \delta_1 = 0$. Left: with the minmod limiter; right: with the smooth limiter (MUSCL 300 points: dash-dot; WENO-Roe 1200 points: solid).

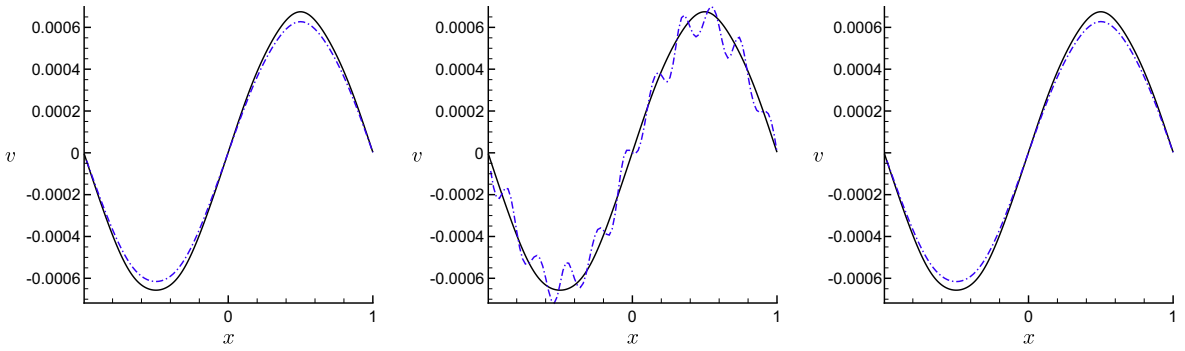

Fig. 6. Small perturbation of velocity results. Perturbation of velocity $\epsilon = 10^{-3} \times \sin(\pi x)$. Dash-dot: left: WENO-Roe 100 points; middle: WENO-LF 100 points; right: hybrid WENO-LF 100 points. Solid: WENO-Roe 1200 points.

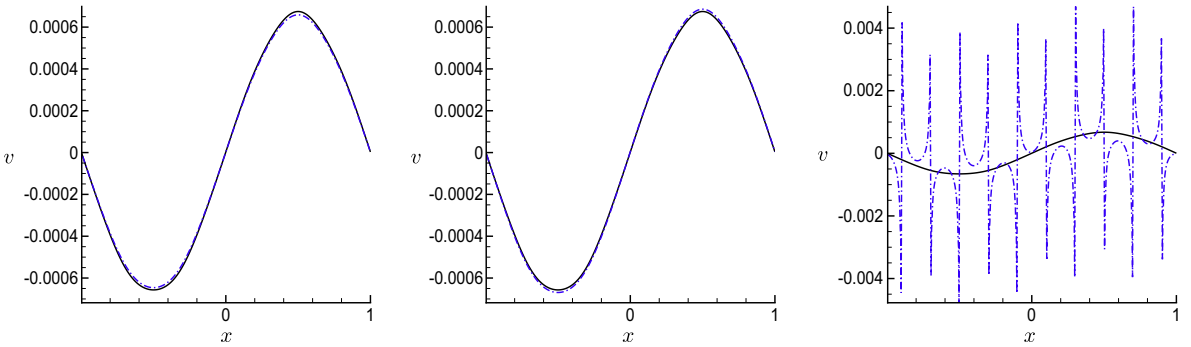

Fig. 7. Small perturbation of velocity results. Perturbation of velocity $\epsilon = 10^{-3} \times \sin(\pi x), \delta_1 = 0$. Dash-dot: left: P–C TVD 200 points; middle: Harten–Yee TVD 300 points; right: MUSCL scheme 600 points. Solid: WENO-Roe 1200 points.

have much bigger oscillations even on a mesh with 600 grid points. The non well-balanced WENO-LF behaves better than the MUSCL scheme, due to the high-order convergence of the former.

Through the examples of perturbations of density, velocity and energy, we clearly demonstrate the advantages of using well-balanced schemes in capturing the small perturbation of steady states.

Nearly well-balanced schemes. Recall in the Section 4.1.1, when the entropy fix parameter δ_1 is non-zero, the last filter step causes trouble, thus P–C TVD and TVD schemes are not well-balanced schemes any more for the steady state solution (52). However, note that the first linear steps of P–C TVD and TVD schemes are still well-balanced. For the sake of this, we call them "nearly well-balanced" schemes, in contrast to the "non well-balanced" MUSCL scheme which is not well-balanced everywhere. Here we will show the advantages of nearly well-balanced schemes through the small perturbation problems.

We perform the same perturbation tests here, but by the non-zero entropy fix parameter schemes. Fig. 10 shows the density plots at $t = 0.1$ under a perturbation of density (57) by P–C TVD, Harten–Yee TVD and MUSCL schemes, respectively. Figs.

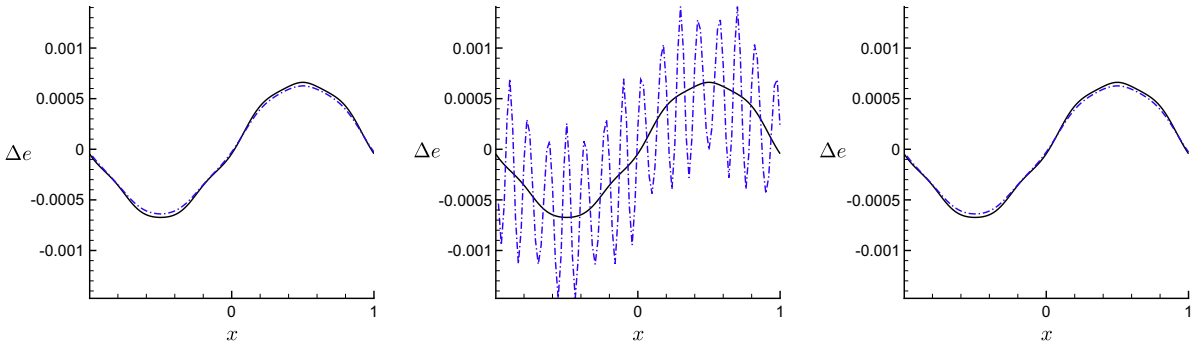

Fig. 8. Small perturbation of energy results. Perturbation of energy $\epsilon = 10^{-3} \times \sin(\pi x)$. Dash-dot: left: WENO-Roe 100 points; middle: WENO-LF 100 points; right: hybrid WENO-LF 100 points. Solid: WENO-Roe 1200 points.

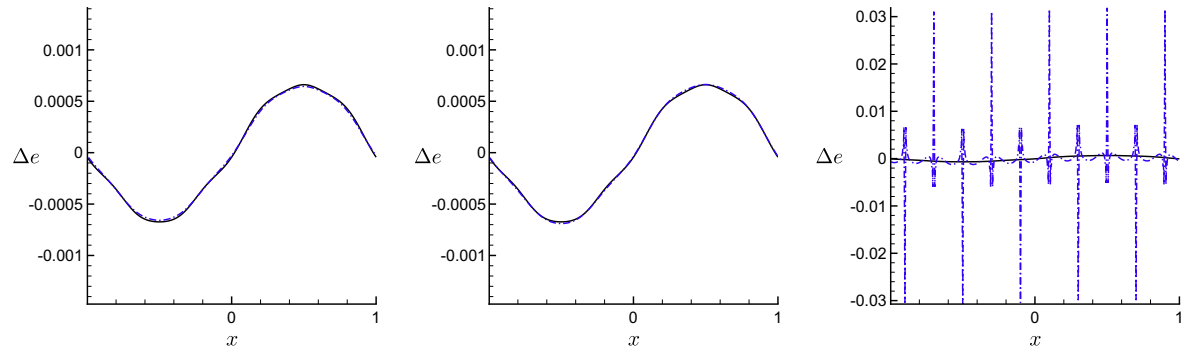

Fig. 9. Small perturbation of energy results. Perturbation of energy $\epsilon = 10^{-3} \times \sin(\pi x), \delta_1 = 0$. Dash-dot: left: P–C TVD 200 points; middle: Harten–Yee TVD 300 points; right: MUSCL scheme 600 points. Solid: WENO-Roe 1200 points.

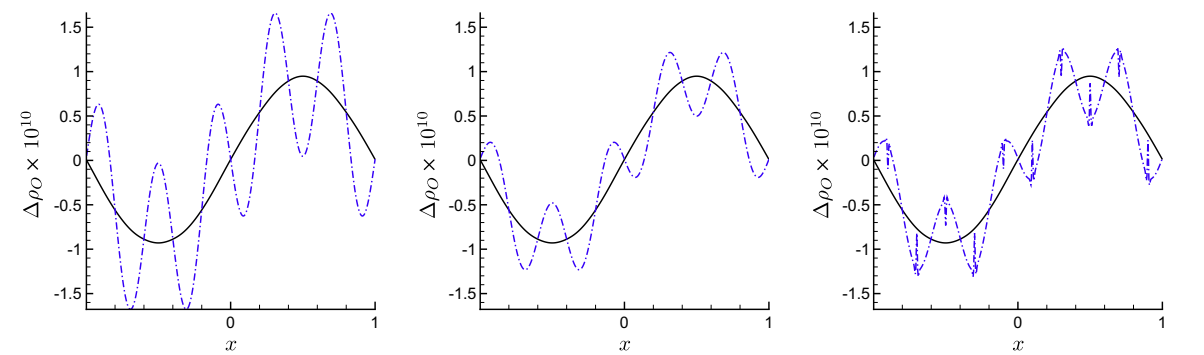

Fig. 10. Non-zero entropy fix parameter results of density ρ_o: perturbation of density $\epsilon = 10^{-10} \times \sin(\pi x), \delta_1 = 0.2$. Dash-dot: left: P–C TVD 600 points; middle: Harten–Yee TVD 600 points; right: MUSCL scheme 600 points. Solid: WENO-Roe 1200 points.

11 and 12 show the velocity and energy plots under a perturbation of velocity (58) and energy (59), respectively. The analysis in Section 4.1.1 indicates that non-zero δ_1 introduces truncation errors in the filter step, which makes P–C TVD and TVD schemes not well-balanced any more. The smaller δ_1 is, the smaller truncation errors it will cause, thus the better performance these schemes will have.

In Figs. 10 and 12, the results by P–C TVD and Harten–Yee TVD schemes have smooth fluctuations, which is due to the truncation error by the entropy fix parameter δ_1. MUSCL does not show big difference between zero δ_1 results (right subplot of Fig. 7) and non-zero δ_1 results (right subplot of Fig. 12) in the perturbation of energy problem (59), because the truncation error caused by δ_1 is much smaller than the original truncation error. MUSCL scheme has error 10 times larger than P–C TVD scheme and Harten–Yee TVD scheme, hence it needs many more points to converge. The nearly well-balanced P–C TVD

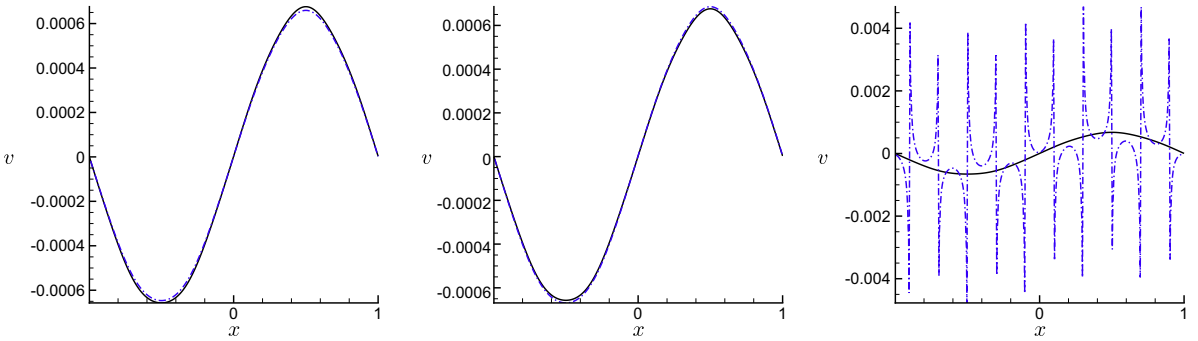

Fig. 11. Non-zero entropy fix parameter results of velocity: perturbation of velocity $\epsilon = 10^{-3} \times \sin(\pi x), \delta_1 = 0.2$. Dash-dot: left: P–C TVD 200 points; middle: Harten–Yee TVD 300 points; right: MUSCL scheme 600 points. Solid: WENO-Roe 1200 points.

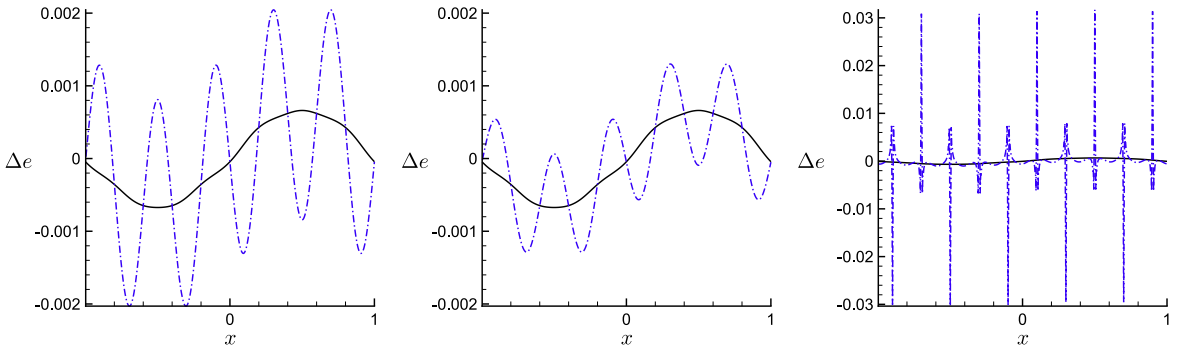

Fig. 12. Non-zero entropy fix parameter results of energy: perturbation of energy $\epsilon = 10^{-3} \times \sin(\pi x), \delta_1 = 0.2$. Dash-dot: left: P–C TVD 600 points; middle: Harten–Yee TVD 600 points; right: MUSCL scheme 600 points. Solid: WENO-Roe 1200 points.

scheme and Harten–Yee TVD scheme still perform better than the non well-balanced MUSCL scheme. This can be seen more clearly from a larger perturbation test, for example,

$$\rho e_0' = \rho e_0 + \epsilon, \tag{60}$$

with $\epsilon = \sin(\pi x)$. The results of energy difference are shown in Fig. 13. In this case, the perturbation is relatively large compared to the truncation error caused by δ_1. Thus we can see that the nearly well-balanced P–C TVD scheme and Harten–Yee TVD scheme are able to resolve this perturbation very well (left and middle subplots of Fig. 13), whereas the non well-balanced MUSCL scheme cannot do it in the same mesh (right subplot of Fig. 13).

Unlike the density and the energy cases, in the perturbation of velocity problem (58), the non-zero δ_1 does not have any influence on the velocities (Fig. 11). This is because the $(n_s + 1)th$ element of $R\Phi$ is always zero as long as the velocity is zero.

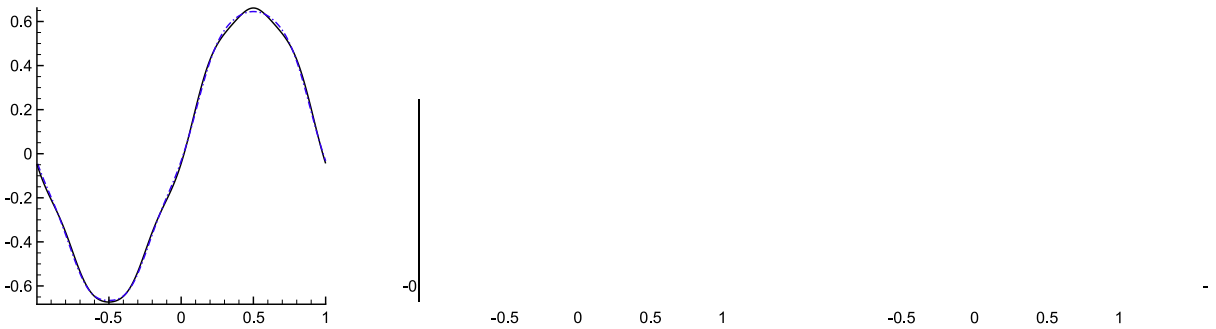

Thus, the velocity plots for P–C TVD scheme and Harten–Yee TVD scheme remain as good as the zero δ_1 case (left and middle subplots of Fig. 7).

4.1.3. A shock tube problem

The third example consists of a shock tube where the high pressure, high-temperature on the left half plane and the low pressure, low temperature on the right plane, both contain air, initially in chemical equilibrium. The conditions are:

$$(p_L, T_L) = (1.003 \times 10^5 \text{ N/m}^2, 4000 \text{ K}), \quad (p_R, T_R) = (0.6 \times 10^5 \text{ N/m}^2, 1800 \text{ K}),$$

with zero velocity everywhere and the densities satisfying Eq. (55). Our well-balanced schemes are balanced for the left and right states individually, but not through the transition. The WENO-Roe, hybrid WENO-LF, Harten–Yee and MUSCL schemes are tested. We want to demonstrate that the well-balanced (or nearly well-balanced) schemes not only behave nicely near the steady state but also can keep good properties far away from steady state, such in non-oscillatory shock-capturing. The

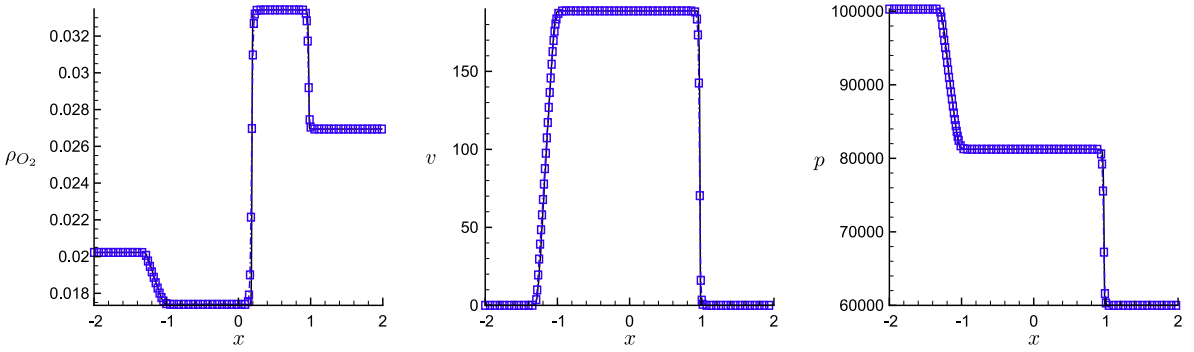

Fig. 14. Riemann problem: left: density; middle: velocity; right: pressure (WENO-Roe 300 points: dash line with symbols; WENO-LF 1200 points: solid).

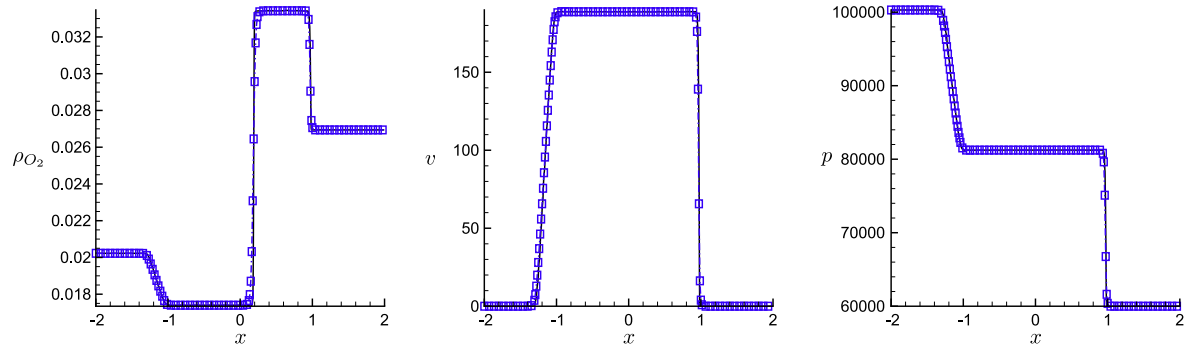

Fig. 15. Riemann problem: left: density; middle: velocity; right: pressure (hybrid WENO-LF 300 points: dash line with symbols; WENO-LF 1200 points: solid).

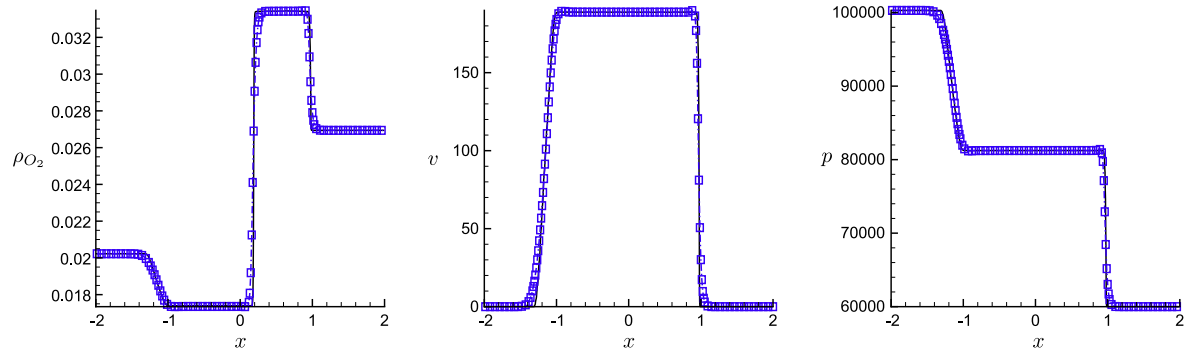

Fig. 16. Riemann problem: left: density; middle: velocity; right: pressure (P–C TVD 300 points: dash line with symbols; WENO-LF 1200 points: solid).

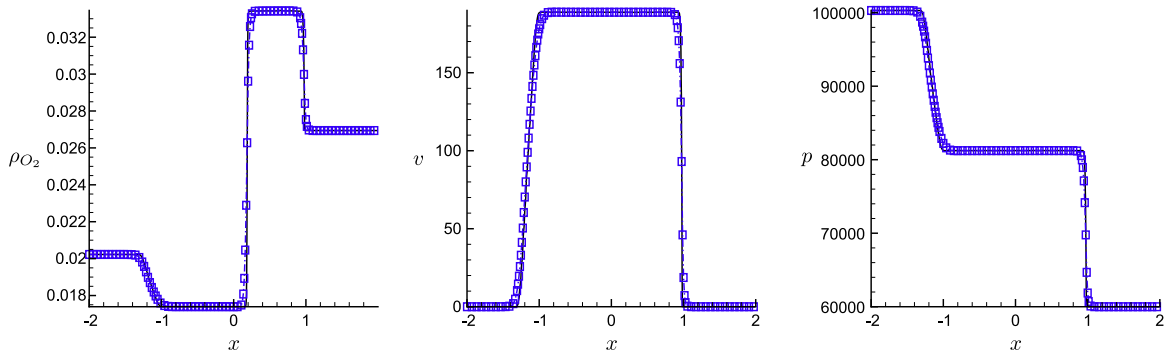

Fig. 17. Riemann problem: left: density; middle: velocity; right: pressure (Harten–Yee TVD 300 points: dash line with symbols; WENO-LF 1200 points: solid).

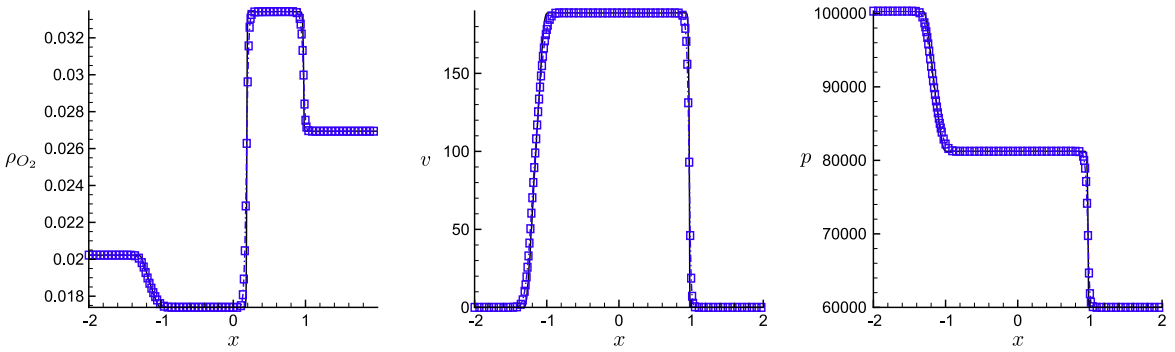

Fig. 18. Riemann problem: left: density; middle: velocity; right: pressure (MUSCL scheme 300 points: dash line with symbols; WENO-LF 1200 points: solid).

reference solution is taken to be regular WENO-LF with 1200 points. The results by WENO-Roe, hybrid WENO-LF, P–C TVD, Harten–Yee and MUSCL schemes at $t = 0.001$ are shown in Figs. 14–18, respectively. For each scheme, density, velocity and pressure are plotted from left to right. The hybrid WENO-LF gives well resolved, non-oscillatory solutions using 300 uniform cells. We can see clearly from these figures that the well-balanced schemes, i.e., WENO-Roe, hybrid WENO-LF, Harten–Yee, have the same non-oscillatory shock-capturing capability as the other schemes.

4.2. Nozzle flow

In this section, the quasi-one-dimensional non-equilibrium nozzle flow with the reaction terms (see the equilibrium nozzle flow [3]) is considered. The governing equations for the non-equilibrium flow with three species $(\rho_1 = O, \rho_2 = O_2, \rho_3 = N_2)$ through a duct of varying cross section can be written in conservation form as:

$$\begin{aligned} &(\rho_i A)_t + (\rho_i v A)_x = s^i A, \quad i = 1, \ldots, 3, \\ &(\rho v A)_t + ((\rho v^2 + p)A)_x = pA'(x), \\ &(\rho e_0 A)_t + ((\rho e_0 + p) v A)_x = 0, \end{aligned} \tag{61}$$

where $A = A(x)$ denotes the area of the cross section and s^i is given by Eq. (47).

4.2.1. Well-balanced test

First the well-balanced properties of our schemes are tested for the same steady state (52), for which the cross section area and the initial conditions are taken as

$$A(x) = 2 + \sin(\pi x), \quad 0 \leqslant x \leqslant 2, \tag{62}$$

$$v(x,0) = 0 \text{ m/s}, \quad p(x,0) = 10^5 \text{ N/m}^2, \quad T(x,0) = 2000 \text{ K}, \tag{63}$$

with periodic boundary conditions. The densities of each species are obtained by the equilibrium state condition $S(U) = 0$ and Eq. (55).

Table 4
L^1 relative errors of ρ_{O_2} for nozzle flow by WENO schemes with N uniform grid points.

N	Error	Order	Error	Order	Error
	WENO-Roe		WENO-LF		Balanced WENO-LF
40	9.78E−06	–	1.81E−05	–	1.01E−14
80	3.08E−07	4.99	5.80E−07	4.96	1.59E−14
160	9.60E−09	5.00	1.81E−08	4.99	3.05E−14
320	2.99E−10	5.01	5.66E−10	5.00	4.04E−14

Table 5
L^1 relative errors of ρ_{O_2} for nozzle flow by TVD schemes with N uniform grid points.

N	Error	Order	Error	Order
	Harten–Yee		MUSCL	
40	1.83E−03	–	6.64E−04	–
80	4.31E−04	2.08	2.47E−04	1.43
160	1.40E−04	1.62	6.90E−05	1.84
320	4.31E−05	1.70	1.88E−05	1.87

The balanced WENO-LF scheme (20) is considered in this section. We take

$$\begin{cases} r_i(U,x) = \rho_i \quad i = 1,\ldots,3, \\ r_4(U,x) = v, \\ r_5(U,x) = p, \end{cases} \tag{64}$$

which achieve constant values for the steady state (63) and thus satisfy the Assumption 1 of the well-balanced condition.

Note that an extra source term $pA'(x)$ in addition to the chemical reaction terms appears in Eq. (61). As stated in Section 3, this term needs special treatment in order to get the well-balanced WENO schemes. First, $pA'(x)$ is written in the form of (15) with $\tau(r(u,x)) = p$ and $t(x) = A(x)$. Then, it is approximated by the same finite-difference operator as that for the flux, i.e., Eq. (18).

Table 4 lists the errors and accuracies of the regular WENO schemes and balanced WENO-LF scheme at $t = 0.01$ (about 3000 time steps for $N = 320$ points). As before, the exact non-trivial steady state solution is known and the relative error is measured between the exact and numerical solutions and then divided by the L_1 norm of the exact solution. As shown in Table 4, none of the regular WENO schemes are well-balanced if just pointwise evaluation is used to the source term. Notice that it is different from the problem in Section 4.1.1, when there is no spatial derivative involved in the source term and the WENO-Roe scheme is well-balanced. We see a clean fifth-order accuracy for the regular WENO schemes. The balanced WENO-LF scheme (20) with special treatment to the source term (18) gives errors at the level of machine round-off errors for double precision, thus it maintains the steady state solution (63) exactly.

Table 5 lists the errors and accuracies of Harten–Yee TVD scheme and MUSCL TVD scheme. Harten–Yee TVD scheme appears to be not well-balanced in this case. Recall the analysis in Section 4.1.1,

$$\alpha^{ns+k} = (\Delta(A(x)p) \pm aA(x)\rho\Delta v)/2a^2 \quad k = 1,2, \tag{65}$$

for the nozzle flow problem Eq. (61). Thus α^{ns+1} and α^{ns+2} are no longer zeros. Both Harten–Yee TVD scheme and MUSCL TVD scheme show a second-order accuracy for the well-balanced test.

4.2.2. Small perturbation

The following test case is chosen to demonstrate the capability of the proposed scheme for computations on the perturbation of the steady state solution (63), which cannot be captured well by a non well-balanced scheme.

A perturbation of density ρ_{O_2} is considered, i.e.,

$$\rho'_{O_2} = \rho_{O_2} + \epsilon, \tag{66}$$

with $\epsilon = 10^{-5} \times \sin(\pi x)$ (about 0.1% of the mean flow). The plot of density ρ_{O_2} at the time $t = 0.05$ is shown in Fig. 19. The regular WENO-LF scheme with $N = 1200$ points is used as a reference solution. The balanced WENO-LF can capture the perturbation very well in a mesh size of only 60 points. However, neither Harten–Yee nor MUSCL scheme can do that in a coarse mesh. Similarly, we perturb the velocity

$$v' = v + \epsilon, \tag{67}$$

with $\epsilon = 0.5 \times \sin(\pi x)$ and the pressure

$$p' = p + \epsilon, \tag{68}$$

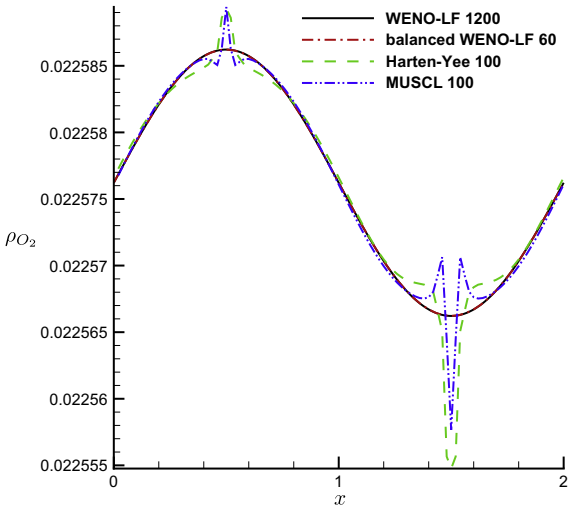

Fig. 19. Small density perturbation of the nozzle flow.

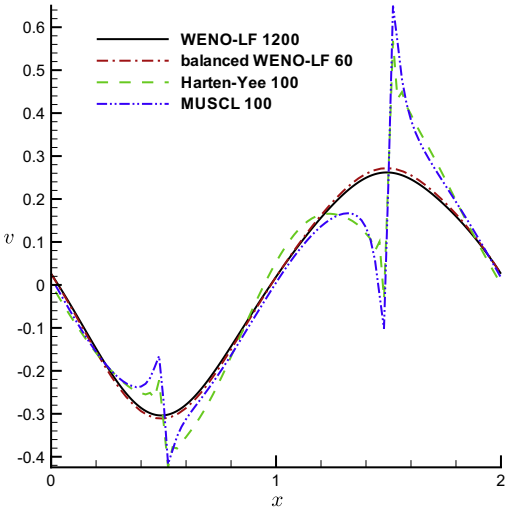

Fig. 20. Small velocity perturbation of the nozzle flow.

with $\epsilon = 10 \times \sin(\pi x)$ separately. The well-balanced WENO-LF scheme again presents good resolution of small perturbations in the plots of velocity (Fig. 20) and pressure (Fig. 21). However, the non well-balanced schemes show spurious oscillations and need more points to resolve the solution.

4.2.3. A shock problem

Proposed by Anderson in [1], it is concerned with a convergent–divergent nozzle flow with a parabolic area distribution, which is given by

$$A(x) = 1 + 2.2(x - 1.5)^2, \quad 0 \leqslant x \leqslant 3. \tag{69}$$

The initial conditions are taken as the equilibrium state of

$$v(x,0) = 0 \text{ m/s}, \quad p(x,0) = 10^5 \text{ N/m}^2, \quad T(x,0) = 2000 \text{ K}.$$

The boundary conditions are taken as one bar of pressure at the left, 0.6784 bar of pressure at the right, and 2000 K of temperature at both ends. The boundary conditions for the density of each species are obtained from the equilibrium conditions at the boundaries. The flow at boundaries are subsonic for both inflow and outflow. A shock is established inside the pipe. The computation is performed using $N = 200$ points to $t = 0.1$. The pressure p and velocity v are plotted.

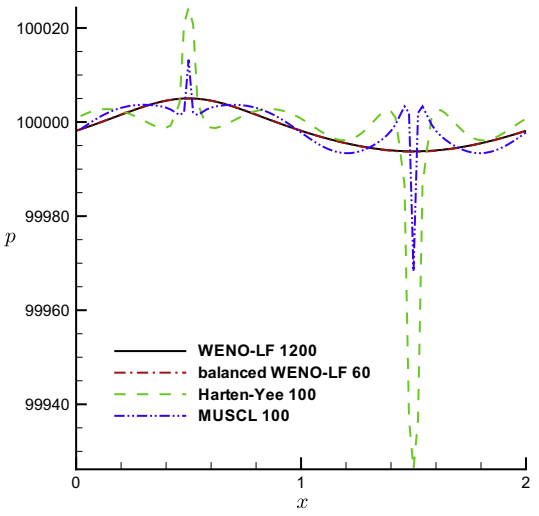

Fig. 21. Small pressure perturbation of the nozzle flow.

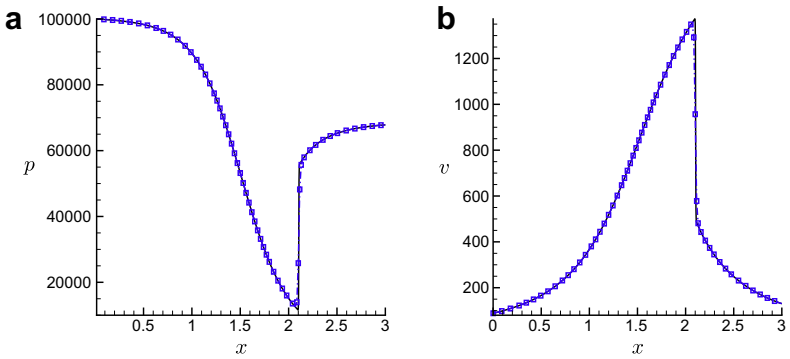

Fig. 22. Nozzle flow: (a) left: pressure; (b) right: velocity (balanced WENO-LF 200 points: dash line with symbols; WENO-LF 1200 points: solid).

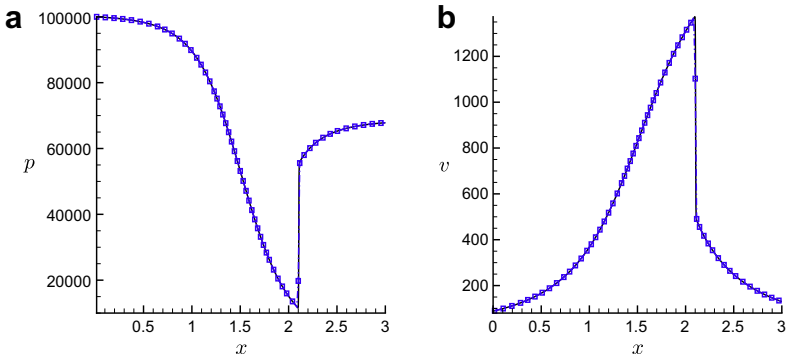

Fig. 23. Nozzle flow: (a) left: pressure; (b) right: velocity (Harten–Yee scheme 200 points: dash line with symbols; WENO-LF 1200 points: solid).

The results by balanced WENO-LF scheme are shown in Fig. 22. The numerical resolution is very good without oscillations, verifying the essentially non-oscillatory property of the balanced WENO-LF scheme. For comparison, the results by Harten–Yee TVD and MUSCL are also presented in Figs. 23 and 24, respectively.

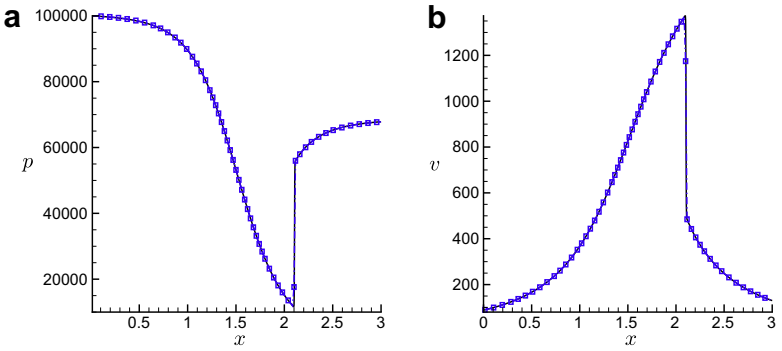

Fig. 24. Nozzle flow: (a) left: pressure; (b) right: velocity (MUSCL scheme 200 points: dash line with symbols; WENO-LF 1200 points: solid).

5. Concluding remarks

The current results serve as a preliminary study on well-balanced schemes for non-equilibrium flow with source terms. The well-balanced WENO schemes are constructed for the non-equilibrium flow. Numerical examples are given to demonstrate the well-balanced property, accuracy, good capturing of the small perturbation to the steady state solutions, and the non-oscillatory shock resolution of the proposed numerical method. Future research will apply the same approach to analyze the well-balanced properties for the model with larger number of species, and for multi-dimensional flows. A more general type of steady state problem with non-zero velocity will also be considered. In this case, the source terms are balanced by the flux gradients. Special attention will be paid to general reactive flows for which perturbation from equilibrium states could be small in some parts of the domain and large in other parts.

Acknowledgments

The authors acknowledge the support of the DOE/SciDAC SAP grant DE-AI02-06ER25796. The work by Björn Sjögreen is performed under the auspices of the U.S. Department of Energy by Lawrence Livermore National Laboratory under Contract No. DE-AC52-07NA27344 LLNL-JRNL-409903.

Appendix A. Additive Runge–Kutta scheme

The implicit time method we are interested in is Additive Runge–Kutta Scheme (ARK) introduced by Kennedy and Carpenter [12].

Rewrite Eq. (2) as

$$\begin{cases} U_t = F_N(t, U(t)) + F_S(t, U(t)), \\ U(0) = U_0, \end{cases} \tag{70}$$

where F_N denotes the non-stiff term and F_S denotes the stiff term.

Table 6
The coefficients for ARK3.

	$j=0$	$j=1$	$j=2$	$j=3$
$a_{ij}^{[N]}$				
$i=1$	$\frac{1767732205903}{2027836641118}$			
$i=2$	$\frac{5535828885825}{10492691773637}$	$\frac{788022342437}{10882634858940}$		
$i=3$	$\frac{6485989280629}{16251701735622}$	$-\frac{4246266847089}{9704473918619}$	$\frac{10755448449292}{10357097424841}$	
$a_{ij}^{[S]}$				
$i=1$	$\frac{1767732205903}{4055673282236}$	$\frac{1767732205903}{4055673282236}$		
$i=2$	$\frac{2746238789719}{10658868560708}$	$-\frac{640167445237}{6845629431997}$	$\frac{1767732205903}{4055673282236}$	
$i=3$	$\frac{1471266399579}{7840856788654}$	$-\frac{4482444167858}{7529755066697}$	$\frac{11266239266428}{11593286722821}$	$\frac{1767732205903}{4055673282236}$
$b_j^{[N]}$	$\frac{1471266399579}{7840856788654}$	$-\frac{4482444167858}{7529755066697}$	$\frac{11266239266428}{11593286722821}$	$\frac{1767732205903}{4055673282236}$
$b_j^{[S]}$	$\frac{1471266399579}{7840856788654}$	$-\frac{4482444167858}{7529755066697}$	$\frac{11266239266428}{11593286722821}$	$\frac{1767732205903}{4055673282236}$
c_j	0	$\frac{1767732205903}{2027836641118}$	0.6	1

Table 7
cfl Numbers based on numerical test.

N	WENO		2nd order TVD schemes	
	RK3	ARK3	RK2	IE2
40	0.002	0.3	0.002	0.3
80	0.004	0.4	0.004	0.4
100	0.004	0.5	0.005	0.4

The ARK scheme to Eq. (70) has the following form

$$U^{(i)} = U^n + \Delta t \sum_{j=0}^{i-1} a_{ij}^{[N]} F_N(t^n + c_j \Delta t, U^{(j)}) + \Delta t \sum_{j=0}^{i} a_{ij}^{[S]} F_S(t^n + c_j \Delta t, U^{(j)}), \tag{71}$$

$$U^{n+1} = U^n + \Delta t \sum_{j=0}^{s} b_j^{[N]} F_N(t^n + c_j \Delta t, U^{(j)}) + \Delta t \sum_{j=0}^{s} b_j^{[S]} F_S(t^n + c_j \Delta t, U^{(j)}), \tag{72}$$

where $U^{(0)} = U^n$ and $U^{(i)}$ approximates $U(t^n + c_i \Delta t), i = 1, \ldots, s$. The non-stiff and stiff terms are integrated by their own $(s+1)$-stage Runge–Kutta methods, respectively.

The coefficients $a_{ij}^{[N]}, a_{ij}^{[S]}, b_j^{[N]}, b_j^{[S]}, c_j$ are constrained by order of accuracy and stability considerations. A third-order ARK method are considered in the computation.

The coefficients for the 3rd order ARK method (ARK3) we use are listed in Table 6. For more details, we refer the readers to [12].

For the second-order schemes such as Harten–Yee and MUSCL, we use a simple second-order implicit–explicit Runge–Kutta scheme (IE2) for the time discretization, which has the form

$$U^{(1)} = U^n + \Delta t F_N(t^n, U^n) + \Delta t F_S(t^n, U^n), \tag{73}$$

$$U^{n+1} = ((U^{(1)} + U^n) + \Delta t F_N(t^{n+1}, U^{(1)}) + \Delta t F_S(t^{n+1}, U^{n+1}))/2. \tag{74}$$

Remark 1. In the steady state or close to steady state problems, the source term is close to zero and thus not stiff. Both an explicit and an implicit time methods can be used. However, away from the steady state, such as the shock problem in 4.1.3, using an implicit time method allows a large cfl number and thus saves computational cost. In Table 7, we list the maximum cfl numbers allowed for WENO scheme and second-order TVD schemes (Harten–Yee and MUSCL) with different time discretizations mentioned in Appendix A. Implicit methods show big advantage of saving computational cost especially in coarse meshes. When the mesh is refined, the source term becomes less stiff.

References

[1] J.D. Anderson, Computational Fluids Dynamics, McGraw-Hill, New York, 1995.
[2] B. Engquist, B. Sjögreen, Robust Difference Approximation for Stiff Inviscid Detonation Waves, Report CAM 91-05, Dept. of Math., UCLA, 1991.
[3] Ll. Gascón, J.M. Corberán, Construction of second-order TVD schemes for nonhomogeneous hyperbolic conservation laws, J. Comp. Phys. 172 (2001) 261–297.
[4] P.A. Gnoffo, R.N. Gupta, J.L. Shinn, Conservation equations and physical models for hypersonic air flows in thermal and chemical nonequilibrium, NASA Technical Paper 2867, 1989, 1–58.
[5] J.M. Greenberg, A.Y. LeRoux, A well-balanced scheme for the numerical processing of source terms in hyperbolic equations, SIAM J. Numer. Anal. 33 (1996) 1–16.
[6] D.F. Griffiths, A.M. Stuart, H.C. Yee, Numerical wave propagation in hyperbolic problems with nonlinear source terms, SIAM J. Numer. Anal. 29 (1992) 1244–1260.
[7] B. Grossman, P. Cinnella, Flux-split algorithms for flows with non-equilibrium chemistry and vibrational relaxation, J. Comp. Phys. 88 (1990) 131–168.
[8] A. Harten, P.D. Lax, B. Van Leer, On upstream differencing and Godunov-type schemes for hyperbolic conservation laws, SIAM Rev. 25 (1983) 35–61.
[9] M.E. Hubbard, P. Garcia-Navarro, Flux difference splitting and the balancing of source terms and flux gradients, J. Comp. Phys. 165 (2000) 89–125.
[10] G. Jiang, C.-W. Shu, Efficient implementation of weighted ENO schemes, J. Comp. Phys. 126 (1996) 202–228.
[11] S. Jin, A steady-state capturing method for hyperbolic systems with geometrical source terms, Math. Modell. Numer. Anal. (M^2AN) 35 (2001) 631–645.
[12] C.A. Kennedy, M.H. Carpenter, Additive Runge–Kutta schemes for convection–diffusion–reaction equations, Appl. Numer. Math. 44 (2003) 139–181.
[13] A. Kurganov, D. Levy, Central-upwind schemes for the Saint–Venant system, Math. Modell. Numer. Anal. (M^2AN) 36 (2002) 397–425.
[14] A. Lafon, H.C. Yee, Dynamical approach study of spurious steady-state numerical solutions for non-linear differential equations, Part III: The effects of non-linear source terms in reaction–convection equations, Comp. Fluid Dyn. 6 (1996) 1–36.
[15] A. Lafon, H.C. Yee, Dynamical approach study of spurious steady-state numerical solutions for non-linear differential equations, Part IV: Stability vs. numerical treatment of non-linear source terms, Comp. Fluid Dyn. 6 (1996) 89–123.
[16] R.J. LeVeque, Balancing source terms and flux gradients in high-resolution Godunov methods: the quasi-steady wave-propagation algorithm, J. Comp. Phys. 146 (1998) 346–365.
[17] R.J. LeVeque, H.C. Yee, A study of numerical methods for hyperbolic conservation laws with stiff source terms, J. Comp. Phys. 86 (1990) 187–210.

[18] S. Noelle, Y. Xing, C.-W. Shu, High order well-balanced finite volume WENO schemes for shallow water equation with moving water, J. Comp. Phys. 226 (2007) 29–58.
[19] T.C. Rebollo, A.D. Delgado, E.D.F. Nieto, A family of stable numerical solvers for the shallow water equations with source terms, Comp. Meth. Appl. Mech. Eng. 192 (2003) 203–225.
[20] M. Ricchiuto, R. Abgrall, H. Deconinck, Application of conservative residual distribution schemes to the solution of the shallow water equations on unstructured meshes, J. Comp. Phys. 222 (2007) 287–331.
[21] M. Ricchiuto, A. Bollermann, Stabilized residual distribution for shallow water simulations, J. Comp. Phys. 228 (2009) 1071–1115.
[22] P.L. Roe, Approximate Riemann solvers, parameter vectors, and difference schemes, J. Comp. Phys. 43 (1981) 357–372.
[23] G. Russo, Central schemes for balance laws, in: Proceedings of the VIII International Conference on Nonlinear Hyperbolic Problems, Magdeburg, 2000.
[24] C.-W. Shu, Essentially non-oscillatory and weighted essentially non-oscillatory schemes for hyperbolic conservation laws, in: A. Quarteroni (Ed.), Advanced Numerical Approximation of Nonlinear Hyperbolic Equations, Lecture Notes in Mathematics, vol. 1697, Springer, 1998, pp. 325–432.
[25] C.-W. Shu, S. Osher, Efficient implementation of essentially non-oscillatory shock-capturing schemes, J. Comp. Phys. 77 (1988) 439–471.
[26] Y. Xing, C.-W. Shu, High order finite difference WENO schemes with the exact conservation property for the shallow water equations, J. Comp. Phys. 208 (2005) 206–227.
[27] Y. Xing, C.-W. Shu, High order well-balanced finite difference WENO schemes for a class of hyperbolic systems with source terms, J. Sci. Comp. 27 (2006) 477–494.
[28] K. Xu, A well-balanced gas-kinetic scheme for the shallow-water equations with source terms, J. Comp. Phys. 178 (2002) 533–562.
[29] H.C. Yee, Construction of explicit and implicit symmetric TVD schemes and their applications, J. Comp. Phys. 68 (1987) 151–179.
[30] H.C. Yee, A class of high-resolution explicit and implicit shock-capturing methods, VKI lecture series 1989-04, March 6–10, 1989; NASA TM-101088, Feb. 1989, 1989.
[31] H.C. Yee, A. Harten, Implicit TVD schemes for hyperbolic conservation laws in curvilinear coordinates, AIAA J. 25 (1987) 266–274.
[32] H.C. Yee, J.L. Shinn, Semi-implicit and fully implicit shock-capturing methods for nonequilibrium flows, AIAA J. 225 (1989) 910–934.
[33] H.C. Yee, B. Sjögreen, Development of low dissipative high order filter schemes for multiscale Navier–Stokes/MHD systems, J. Comp. Phys. 68 (2007) 151–179.
[34] H.C. Yee, P.K. Sweby, D.F. Griffiths, Dynamical approach study of spurious steady-state numerical solutions for non-linear differential equations, Part I: The dynamics of time discretizations and its implications for algorithm development in computational fluid dynamics, J. Comp. Phys. 97 (1991) 249–310.
[35] J.G. Zhou, D.M. Causon, C.G. Mingham, D.M. Ingram, The surface gradient method for the treatment of source terms in the shallow-water equations, J. Comp. Phys. 168 (2001) 1–25.